Thermal Management of Batteries Using a Hybrid Supercapacitor Architecture

Donghwa Shin, Massimo Poncino, and Enrico Macii
Dipartimento di Automatica e Informatica, Politecnico di Torino
C.so Duca degli Abruzzi 24, 10129 Torino (ITALY)
{donghwa.shin, massimo.poncino, enrico.macii}@polito.it

Abstract—Thermal analysis and management of batteries have been an important research issue for battery-operated systems such as electric vehicles and mobile devices. Nowadays, battery packs are designed considering heat dissipation, and external cooling devices such as a cooling fan are also widely used to enforce the reliability and extend the lifetime of a battery. This type of approaches that target the enhancement of the cooling efficiency via the reduction of the thermal resistance cannot achieve an immediate temperature drop to avoid a thermal emergency situation. Approaches based on removing the heat from the heat sources via idle period insertion (similar to what is done for silicon devices) would allow faster thermal response; however it is not obvious how to implement these schemes in the context of batteries.

In this paper, we propose the use of a simple parallel battery-supercapacitor hybrid architecture with a dual-mode discharging strategy that can provide immediate temperature management, in which the supercapacitor is used as an energy buffer during the idle periods of the battery. Simulation results shows that the proposed method can keep the battery temperature within the safe range without external cooling devices while exploiting the advantage of the battery-supercapacitor parallel connection.

I. INTRODUCTION

Batteries are the most important energy source for the modern off-the-grid electric or electronic systems and their use is continuosly increasing due to the need of energy storage elements required by new application domains such as renewable energy systems and electric vehicles. The lifetime and the efficiency of a battery is largely affected by its operating temperature; the state-of-health (SOH)[1] of the battery exposed to high temperature is seriously degraded. As an example, it is reported that the SOH of battery in the electric vehicles in a desert is 12% less than the vehicles in temperate climate regions after 10 years [1]. The battery generally needs to be cooled down during discharging period, and also, sometimes, to be heated for the discharging efficiency in a cold condition.

Moreover, batteries are exposed to danger of thermal runaway where themselves also generate the heat during discharging process. Thermal runaway happens when an uncontrolled positive feedback loop is formed between the heat generation and temperature, which is often leading to a destructive result. Thermal runaway of lithium-ion batteries have been reported in cellphones and laptop computers occasionally. The basic solution is to use less reactive electrode materials and non-flammable electrolytes, but it is clear that the operating condition also should be maintained properly.

In general, we can have two categories of active thermal management methods: *thermal resistance*[2]*control* and *heat-source control* [2]. The first category attempt at improving how the heat is removed. For instance, modern microprocessors can be cooled down by using a heat sink and forced-convection cooling devices such as an electric fan or a coolant pump. The fan or pump enhance the heat-transfer efficiency (i.e., reduce the thermal resistance) by increasing the amount of coolant fluid through the heat-exchange channel.

A problem with these approaches is that the cooling device used for the forced convection also consumes substantial amount of power; for instance, in the case of fans, their power consumption is proportional to the cubic of fluid velocity [3]. Another critical limit of the thermal resistance control is that it cannot respond to a sudden temperature drop to avoid a thermal emergency unless it can suddenly change the thermal resistance in a thermal equilibrium. Heat source control methods, conversely, act directly on the generation of heat rather than just removing it; this is typically done by inserting idle periods during system operations. While this is quite standard for digital components, it is apparently not obvious how it could be implemented for energy storage devices.

As a matter of fact, batteries have no equivalent of the power/performance states of digital devices; moreover supply of energy cannot be simply suspended as done for computation: when a battery is disconnected, the system will be shut-down. To avoid this, we need an energy buffer that powers the system while idle periods are inserted into the battery discharging profile. Such energy buffer could be a redundant battery, but this is not a very practical solution in terms of cost and form factor. Furthermore, the redundant battery will undergo the same thermal problem.

The ideal storage buffer should have the following characteristics: i) have large enough energy capacity to cover the idle period, ii) have much lower internal resistance than the battery (less ohmic heat-generation, thus not subject to thermal problems), and iii) allow high number of charge/discharge

[1]A normalized effective capacity of the battery after multiple charge-discharge cycles

[2]The reciprocal of thermal conductance.

cycles (higher than batteries) in order to make the frequent charging-discharging operation possible.

The most suitable candidate for the energy buffer device satisfying that requirements is an electric double-layer capacitors, or simply supercapacitors, the supercapacitors have extremely low internal resistance and virtually unlimited cycle number compared to the battery [4], and have been widely adopted into various hybrid energy storage systems. Even the simplest hybrid architecture - a parallel connection - have been reported to have significant advantage in terms of cycle efficiency.

In this paper, we propose a smart way of using the supercapacitor in the battery-supercapacitor parallel connection. The proposed dual-mode battery-supercapacitor hybrid architecture enables immediate temperature control of the batteries while exploiting the advantage of the parallel connection. We show the feasibility of the proposed hybrid architecture and present a control policy to properly configure what storage device is connected to the load and when, depending on temperature and the respective state of charge (SOC) of the storage devices with a realistic load condition on a electric vehicle.

II. RELATED WORK

Thermal analysis and management of batteries have been an important research issue for electric vehicles. An effect of temperature on SOH degradation in the electric vehicles was analyzed in [5]. A simulation model to evaluate the effect of thermal management on battery life was presented in [6]. Battery pack designs was also investigated in terms of electrochemistry and fluid dynamics in [7]. A pre-heating method as well as a cooling method for the battery in cold climate was introduced in [8]. The requirement for the battery cooling method considering a climate condition was presented in [1].

Supercapacitors are gaining more attention as an electrical energy storage element in various applications thanks to its high cycle efficiency and long lifetime properties. Several battery-supercapacitor hybrid architectures for the hybrid energy systems have been proposed in the literature. A bidirectional converter based approach was introduced for equipped with electric vehicles regenerative braking [9]. An analysis of the hybrid system considering operating conditions and supercapacitor configuration was performed in [10].

The most basic, yet effective, hybrid architecture is a supercapacitor and a battery in parallel. It supports a higher rate of discharging power thanks to the high power density of the supercapacitor, and thus, enhances the discharging efficiency under load fluctuations [11]: the supercapacitor behaves in fact as a filter that relieves peak stresses on the battery. The supercapacitor also serves a thermal management function by reducing the current-induced heat generation at the internal resistance of the batteries, though this is just a side effect. To the best of our knowledge, there have been no attempt to use the hybrid architecture in terms of thermal management so far. The supercapacitors have been only used to enhance the power capacity and cycle efficiency as a power buffer or a load fluctuation filter.

III. BATTERY MODEL

A. Thermal model

(a) Thermal circuit model for unit cell (b) Thermal RC network model for battery pack
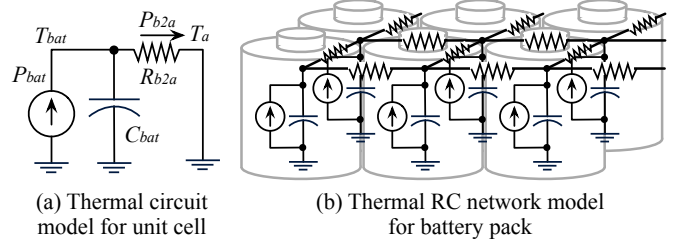
Fig. 1. (a) Lumpled RC-thermal circuit model for unit cell and (b) Thermal RC network model for battery pack.

1) Unit cell model: Figure 1 (a) shows a thermal RC-model used for an unit battery cell in this work. We adopt the heat generation model from [12], which provides reasonable approximation as a function of temperature and charging/discharging current. Heating of a Li-ion battery is calculated from the ohmic power dissipation and the entropy change. The battery current incurs IR drop power losses due to the internal resistance of the batteries, which should be dissipated in the form of heat. At the same time, the charging and discharging of the Li-ion batteries incur entropy change-induced heat. The heat from the battery, P_{bat}, is given by:

$$P_{bat} = I_{bat}(E_{oc} - V_{bat} + T_{bat}\frac{dE_{oc}}{dT_{bat}}),\qquad(1)$$

where I_{bat}, E_{oc}, V_{bat}, and T_{bat} are battery discharging current, open-circuit potential of battery, terminal voltage, and temperature of the battery, respectively. Note that $\frac{dE_{oc}}{dT_{bat}}$ represents the entropy related part, which varies with the battery materials.

The heat generated in the battery flows to the ambient through the thermal resistance, which is determined by the effective surface area and material characteristics. The temperature changes according to the potential of the thermal capacity that is determined by the mass of the battery. We consider the battery as a lumped mass (Figure 1-(a)), with uniform temperature distribution inside and heat flow only at the surface of mass. This simplifcation is acceptable given the small temperature gradient and the small size of the example battery used in this work, that is the Sony US-18650 [13].

P_{bat} increases the temperature of the battery mass or is transferred to the ambient air, which is given as the lumped RC-thermal circuit model:

$$P_{bat} = C_{bat}\frac{dT_{bat}}{dt} + \frac{T_{bat} - T_{amb}}{R_{b2a}},\qquad(2)$$

where T_{bat}, T_{amb}, C_{bat}, and R_{b2a} represent battery temperature, ambient temperature, thermal capacity of the battery, and thermal resistance between battery and ambient air, respectively. C_{bat} is defined as follows.

$$C_{bat} = \rho_c V_c C_{p,c} + \rho_a V_a C_{p,a} + \rho_s V_s C_{p,s},\qquad(3)$$

where $\rho_{\{c,a,s\}}$, $V_{\{c,a,s\}}$, and $C_{p,\{c,a,s\}}$ represent density, volume, and specific heat capacity of cathode, anode, and separator, respectively. Thermal resistance R_{b2a} is calculated from a heat-transfer coefficient, h, and the surface area, A_s ($R_{b2a} = 1/(h \cdot A_s)$). We use physical and chemical parameters for the Sony US-18650 Li-ion battery reported in [14] (Table I).
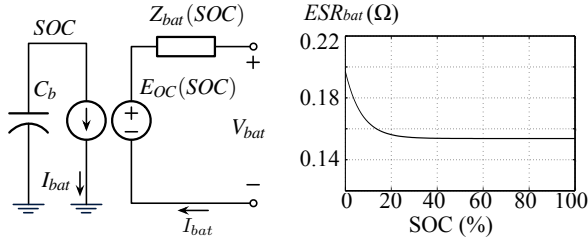
(a) Li-ion battery equivalent circuit model.

(b) Equivalent ESR vs. SOC.

Fig. 2. (a) Li-ion battery circuit model and (b) internal resistance vs. SOC.

2) Battery pack thermal model: In practice, the battery cells are organized in series and parallel connection (a battery pack) to meet the power and energy requirement of the load applications. We built a thermal RC network model based on the unit lumped circuit model, which is widely used to analyze the thermal behavior of the system with laterally connected multiple heat sources [15]. We consider the lateral dependency among the cell by putting the thermal resistances in three dimensional manner as illustrated in Figure 1(b). Note that we do not consider the air flow through the pack, and the thermal resistances for each direction are obtained from R_{b2a} according to the surface area portion of each direction.

B. Electrical model

In order to obtain E_{oc} and V_{bat}, we need an electrical circuit equivalent model of the battery. To accurately estimate the battery temperature, we should use a SOC-related potential and impedance model. An equivalent circuit model considering E_{oc} and equivalent resistance, ESR_{bat}, as a function of the SoC value, SOC, is introduced in [16] as shown in Figure 2.

Note that we use the equivalent resistance of internal impedance, $Z(SOC)$, to calculate the ohmic heat generation in the battery. E_{oc} and ESR_{bat} are given by the following non-linear equations:

$$E_{oc} = b_{11}e^{b_{12}C_{SOC}} + b_{13}SOC^4 + b_{14}SOC^3 + \quad (4)$$
$$b_{15}SOC^2 + b_{16}SOC + b_{17},$$

$$ESR_{bat} = b_{21}e^{b_{22}SOC} + b_{23}, \quad (5)$$

where b_{ij} are empirically-extracted regression coefficients. We extract the b_{ij} from the datasheet of the Sony US-18650 Li-ion battery [17] according to the extraction method presented in [18].

C. Temperature-induced capacity fade of Li-ion battery

A capacity fade (SOH degradation) phenomena is widely reported for various kind of batteries [19]. The capacity fade of Li-ion batteries is often modeled by an Arrhenius type of equation as a function of discharging current, temperature, and the number of cycles [20]. We use the capacity fade during cycling to evaluate the temperature management method in this paper. The capacity fade during cycling is presented as an integration of the following function over time.

$$Q_{loss} = A \cdot e^{-B/(RT)} \cdot I_{bat}^C \quad (6)$$

where R and T are the ideal gas constant and temperature of battery. The coefficient A, B, and C are obtained by regression

TABLE I
PARAMETERS FOR THE BATTERY MODELS.

Thermal model			
Parameter	Value	Parameter	Value
ρ_c	1.622 g/cm^3	V_c	5.61 cm^3
ρ_a	3.115 g/cm^3	V_a	4.88 cm^3
ρ_s	0.946 g/cm^3	V_s	1.35 cm^3
$C_{p,c}$	0.623 J/g/K	$C_{p,a}$	0.601 J/g/K
$C_{p,s}$	1.925 J/g/K	h	35 W/m^2/K
A_s	4.18×10^{-3} m^2	$\frac{dE_{oc}}{dT_{bat}}$	0.00022
Electrical model			
Parameter	Value	Parameter	Value
b_{11}	-0.2653	b_{12}	-61.6492
b_{13}	-2.0398	b_{14}	5.2765
b_{15}	-4.1733	b_{16}	1.6544
b_{17}	3.3564	b_{21}	0.0435
b_{22}	-14.2753	b_{23}	0.1537
Capacity fade model			
Parameter	Value	Parameter	Value
R	8.3144621	A	1.1443×10^6
B	4.257×10^4	C	0.55

analysis of a manufacturer's data. The parameters for the models are summarized in Table I.

IV. DUAL-MODE OPERATION OF SUPERCAPACITOR HYBRID ARCHITECTURE

A. Dual-mode architecture

We propose a dual-mode supercapacitor hybrid architecture to enhance the advantage of the parallel connection in terms of the thermal management. The Li-ion batteries should equips protection circuit to keep them from over-charging or over-discharging. These protection circuits are basically set of switches and bypassing resistors to steering the current [21]. The supercapacitors also usually equip switch-included circuit for cell balancing or overvoltage protection [22]. We will utilize these switches to change the connections between the battery and supercapacitor.

The proposed architecture can be operated in dual-mode: *Parallel mode and switching mode.* The basic idea is to connect the supercapacitor in parallel for efficiency in ordinary state, and use it as a temporal energy buffer to insert an idle period of the batteries when a thermal problem is expected. Figure 3 shows the proposed hybrid architecture. The battery and supercapacitor can be connected in parallel, or connected to the power converter separately by controlling the switches.

The parallel mode operation is the same as the conventional parallel connection battery-supercapacitor. In the switching mode, the supercapcitor and battery is separately connected to the power converter, and during the battery idle periods, the supercapacitor temporarily supplies power to the converter.
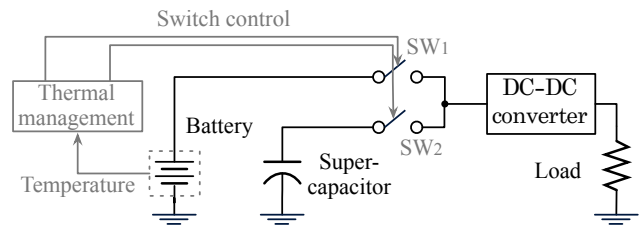
Fig. 3. Proposed dual-mode battery-supercapacitor hybrid architecture for temperature management.
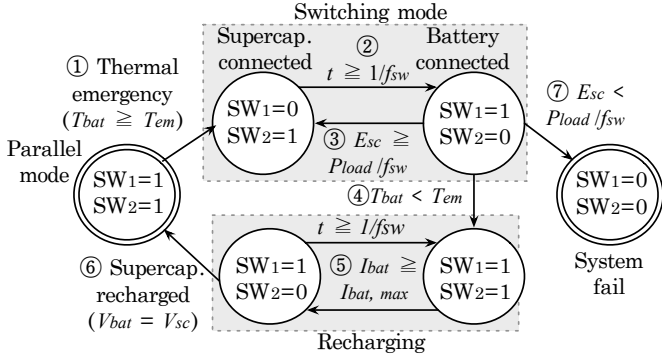
Fig. 4. Control policy of the proposed dual-mode hybrid architecture.

Fig. 5. Estimated battery cycle efficiency and average temperature with different sizes of supercapacitor in parallel for US06 driving profile.

As a result, the battery is immediately cooled down without internal heat generation. Note that the thermal contribution of the supercapacitors is ignored in the experiment where the internal resistance of the supercapacitor is hundreds of times smaller than that of batteries [23].

B. Control policy

Figure 4 shows the state diagram of the controller that regulates the transition between the modes. At first, the battery and supercapacitor are connected in parallel and charged up to the same voltage in the parallel mode. Note that the charging process of the battery is a virtually completely controlled process compared to the discharging process. In this sense, we are focusing on the discharging process, and assume that the battery and supercapacitor are given in charged state to the same voltage.

The specific operation modes are described as transitions in Figure 4 ① – ⑦. The system normally operates in parallel mode (leftmost state in Fig. 4). The battery switch (SW_1) and supercapacitor switch (SW_2) are connected. once T_{bat} becomes greater or equal to the emergency temperature T_{em}, then the battery is disconnected and the operating mode is change to the switching mode (①). SW_1 is disconnected and SW_2 is connected during an idle period, which is derived from pre-determined power gate switching frequency, f_{sw}. After the thermal idle period, the battery is re-connected and the supercapacitor is disconnected during the same period (②). If T_{bat} is still higher than T_{em} and the supercapacitor energy (E_{sc}) is enough for the required energy of next thermal idle period, then another idle period is inserted (③). Otherwise, the controller goes to the fail state and the both of switches are disconnected (⑦).

If T_{bat} drops lower than T_{em}, then the battery and supercapacitor are connected and the supercapacitor is re-charged to switch back to parallel mode (④). The battery current, I_{bat}, is limited by switching of SW_2 lower than the pre-determined maximum current $I_{bat,max}$ (⑤). The operating mode is changed again to the parallel mode when the supercapacitor is charged up to the same voltage of the battery (⑥).

V. CASE STUDY: HYBRID SYSTEM DESIGN AND OPTIMIZATION FOR ELECTRIC VEHICLES

A. Electric vehicle specification and driving profile

We perform the design space exploration of the proposed architecture with a standard driving schedule of the vehicles:
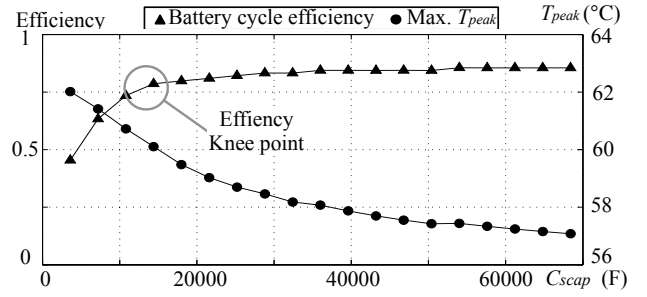
EPA US06 test procedure [24]. The power profile of the electric vehicles with the driving schedule is obtained from a vehicle simulator named ADVISOR, which provides whole vehicle-level simulation with the standard test driving schedules [25]. We use the default configuration of electric vehicle (ev_default_in) provided in ADVISOR.

The battery pack in the target vehicle has 12 V output voltage and 25 kW power capacity. We uses $60 \times 20 \times 3$ battery pack with the Sony US-18650 battery as an unit battery to meet the capacity and voltage. We consider the lateral thermal dependency among the cells in the battery pack with the model presented in Section III-A2. The temperature is calculated by the SPICE simulation of RC-thermal circuit. Note that the target vehicle model does not provide regenerative braking.

B. Design space exploration of hybrid setup

1) Size of supercapacitor: The capacity of energy buffer is determined by the size of the supercapacitor and the input range of the power converter. We can utilize the energy in the supercapapcitor as long as the terminal voltage of the supercapacitor remains within the input range of the DC-DC converter. It is generally expected that large supercapacitor boosts the power capacity of the hybrid system and reduces the load fluctuation more effectively. However, we cannot increase the size of supercapacitor as we want where the volumetric energy density and cost of supercapacitor limit the size of supercapacitor in the hybrid system. As a result, the energy portion of the supercapacitor in the battery-supercapacitor hybrid system is typically just few percent of battery energy [26].

Figure 5 shows the estimation result of battery cycle efficiency (charging-discharging) and peak temperature, T_{peak}, with different size of supercapacitor (C_{scap}) in parallel. T_{peak} is defined as the highest temperature among the cells in a pack, which is used for the controller input. We use the target load profile and battery pack specification introduced in Section V-A for the evaluation. As C_{scap} increasing, the relative effect on temperature is decreasing. The cycle efficiency keeps increasing at the same time, but there is a knee point in the efficiency curve. We will explore the hybrid setups that have capacitance value around the efficiency knee point (5000 F to 25000 F) in the experiment, which can be regarded as a reasonable range (0.4% to 2% of the battery energy). Note that we optimize the size of supercapacitor in the parallel connection in terms of efficiency, and then try to use the supercapacitor for thermal management where a parallel connection is widely adopted architecture. In this paper, we
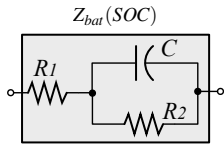
Fig. 6. Battery internal impedance model.

focus on the advanced operating policy of existing parallel connection architecture to utilized the supercapacitors for the thermal management.

2) Power source switching frequency: Concerning idle period insertion, we can leverage some results from the model and literature.

Observation 1: The heat generation model presented in (1) is convex with respect to the current where the heat is proportional to the square of the current. In terms of the heat generation, we should prefer less fluctuated current profile. Therefore, *it is better to use a higher switching frequency that can be filtered by impedance to reduce the fluctuation* where the impedance of the battery acts like a low-pass filter.

Observation 2: The switching of the power gates incurs extra power consumption being proportional to the switching frequency, which is given by $P_{sw} = C_g V_{gs}^2 f_{sw}/2$ where C_g, V_{DD}, and f_{sw} represent effective gate capacitance, gate driving voltage, and the switching frequency of the switch, respectively [4].

The observations 1 and 2 present a tradeoff between the ohmic heat and switching power loss related to f_{sw}. We optimize the switching frequency based on the analysis of the battery heat and switching power loss. We use a typical model of the battery impedance, Z_{bat}, as a set of RC elements as shown in Fig. 6 [27]. It is reported that target battery has a value of 110 mΩ, 40 mΩ, and 4 F for R_1, R_2, and C on average during 1 C discharging, respectively. The parameters of SiR422DP N-channel MOSFET switch are used to calculated the switching power loss P_{sw} [28]. We use 2C amplitude, 50% duty pulsed discharge as a pulsed load, and from 0.1 Hz to 100 Hz switching frequencies are applied.

The estimated power loss in the battery internal resistance and switching power loss are presented in Figure 7. As illustrated in Figure 7 (b), 8 Hz is the lowest frequency that has no additional effect on P_{bat} (heat generated from the battery). The switching power loss with 8 Hz switching frequency is about 0.26 μW, which is a negligible value compared to the

(a) P_{bat} and P_{sw} with different switching frequency

(b) $\Delta P_{bat}/\Delta P_{sw}$ with different switching frequency
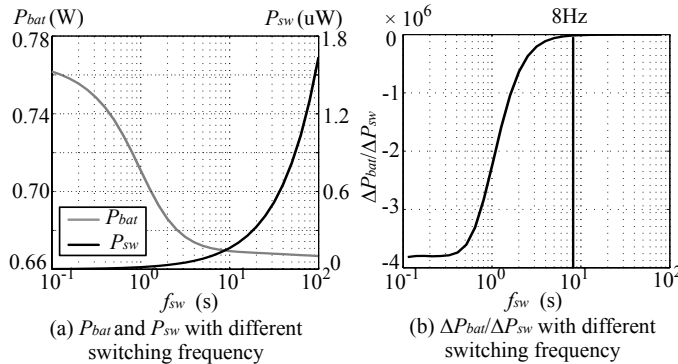
Fig. 7. (a) P_{bat}, P_{sw} and (b) $\frac{\Delta P_{sw}}{\Delta P_{sw}}$ with difference switching frequency.

TABLE II
DISCHARGING TIME OF THE PARALLEL CONNECTION AND THE DUAL-MODE OPERATION WITH DIFFERENT T_{em} AND C_{scap}.

T_{em} (°C)	Simulation results	C_{scap} (F)				
		5000	10000	15000	20000	25000
64	t_{dchg}^{parl} (s)	2702	2725	2982	2982	2983
	t_{dchg}^{dual} (s)	2702	2725	2982	2982	2983
	Extension (%)	-	-	-	-	-
62	t_{dchg}^{parl} (s)	2702	2725	2732	2735	2739
	t_{dchg}^{dual} (s)	2702	2725	2982	2982	2983
	Extension (%)	-	-	9.1	9.0	8.9
60	t_{dchg}^{parl} (s)	2131	2134	2201	2724	2726
	t_{dchg}^{dual} (s)	2136	2735	2982	2982	2983
	Extension (%)	0.2	28.2	35.5	9.5	9.4
58	t_{dchg}^{parl} (s)	2120	2123	2125	2126	2132
	t_{dchg}^{dual} (s)	2125	2705	2784	2982	2983
	Extension (%)	0.2	27.4	31.0	40.3	39.9
56	t_{dchg}^{parl} (s)	1534	1584	1617	2103	2120
	t_{dchg}^{dual} (s)	1607	2124	2722	2983	2983
	Extension (%)	4.4	34.1	68.4	41.8	40.7

total amount of battery power ($\approx$ 4.2V$\times$1.6A = 6.4W). We use 8 Hz as f_{sw} in the experiment based on this result. Note that the IR loss in the switches is relatively huge compared to the swatching loss, but it is the same as the loss due to the protection circuits. We do not consider IR loss as overhead where it is not newly introduced by the proposed method.

C. Experimental result

Table II summarizes the discharging time of the parallel connection (t_{dchg}^{parl}) and dual-mode operation (t_{dchg}^{dual}) with different T_{em} and C_{scap}. We use 5000 F to 25000 F of supercapacitor and 8 Hz f_{sw} according to Section V-B. It shows stepwise aspect due to the periodic characteristics of the load profile. In general, the larger C_{scap} extends the longer discharging time even with the lower T_{em}. With high enough T_{em} (64°C), the parallel connection shows the same performance with the dual-mode operation. However, the proposed dual-mode operation significantly extends the discharging time for lower T_{em} (up to 68.4% with 56 °C as T_{em}).

Fig. 8 shows the temperature and current profile of the conventional parallel connection and proposed dual-mode operation when T_{em} is with 56 °C and C_{scap} is 20000 F. T_{peak}^{parl} and T_{peak}^{dual} represent the highest temperature in the battery pack with the parallel connection and dual-mode operation. t_{dchg}^{dual} is 41.8% longer than t_{dchg}^{parl}, where T_{peak}^{parl} meets T_{em} at 2103 s, and T_{peak}^{dual} meets T_{em} at 2983 s, respectively. Before 2103 s, both of profiles are the same.

T_{peak}^{parl} presented in Fig. 8 ① shows what will happen when we discharge the battery in the parallel connection after the thermal emergency. T_{peak}^{parl} keeps rising up to 62.9 °C while T_{peak}^{dual} is maintained under 56 °C (Fig. 8 ②) by the idle periods inserted in Fig. 8 ③. If we continue to discharge the battery in the parallel connection, it results in extra capacity fade compared to the dual-mode even for the same discharging time. The estimated capacity fade of the dual-mode operation is 14.88% less than that of the parallel connection by (6). Table III shows the estimated capacity fade reduction when
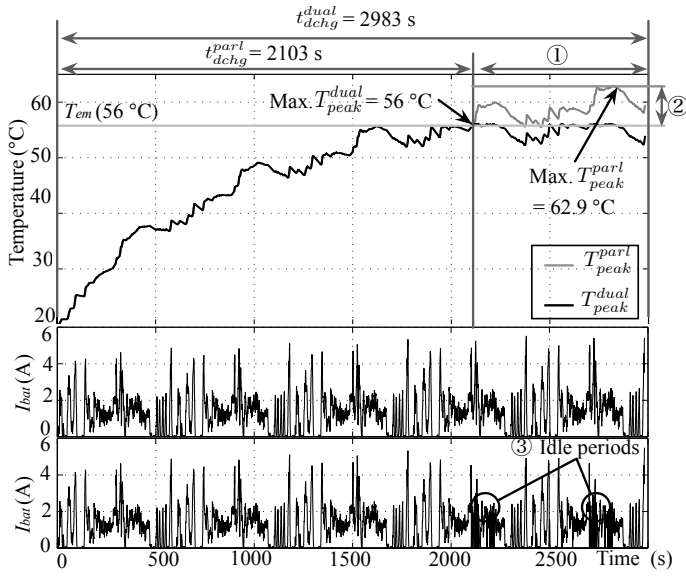
Fig. 8. Current and temperature profile of the battery pack with US06 driving schedule thermal idle period-inserted battery-supercapacitor hybrid.

we discharge the parallel connection and dual-mode for the same time (t_{dchg}^{dual}) in Table II. The maximum difference of T_{peak}^{parl} and T_{peak}^{dual} is up to 6.9°C, and the proposed method reduces the capacity fade up 14.88% by maintaining the temperature under T_{em}.

VI. CONCLUSION

In terms of the efficiency and reliability, the battery-supercapacitor hybrid system has significant advantages. The supercapacitors have been used as a power buffer or a load fluctuation filter for the efficiency so far. On the other hand, we can also use the supercapacitors in the hybrid systems as an energy buffer to insert the thermal idle periods. In this paper, we propose a dual-mode hybrid architecture for the battery and supercapacitor, which can make immediate temperature

TABLE III
PEAK TEMPERATURE OF THE PARALLEL CONNECTION AND THE
DUAL-MODE OPERATION WITH THE SAME DISCHARGING TIME.

T_{em} (°C)	Simulation results	C_{scap} (F)				
		5000	10000	15000	20000	25000
64	T_{peak}^{parl} (°C)	61.6	61.5	63.5	62.9	62.5
	T_{peak}^{dual} (°C)	61.6	61.5	63.5	62.9	62.5
	Q_{loss} reduction (%)	-	-	-	-	-
62	T_{peak}^{parl} (°C)	61.6	61.4	63.5	62.9	62.5
	T_{peak}^{dual} (°C)	61.6	61.4	62.0	62.0	62.0
	Q_{loss} reduction (%)	-	-	2.15	1.4	0.74
60	T_{peak}^{parl} (°C)	60.9	61.4	63.5	62.9	62.5
	T_{peak}^{dual} (°C)	60.0	60.0	60.0	60.0	60.0
	Q_{loss} reduction (%)	1.24	2.44	5.53	4.28	3.64
58	T_{peak}^{parl} (°C)	59.2	61.0	63.2	62.9	62.5
	T_{peak}^{dual} (°C)	58.0	58.0	58.0	58.0	58.0
	Q_{loss} reduction (%)	1.50	6.81	9.21	9.65	8.55
56	T_{peak}^{parl} (°C)	56.6	58.4	60.5	62.9	62.5
	T_{peak}^{dual} (°C)	56.0	56.0	56.0	56.0	56.0
	Q_{loss} reduction (%)	1.53	4.45	11.31	14.88	13.75

change of the battery while exploiting the advantage of the conventional battery-supercapacitor parallel connection.

We propose a control policy for the proposed dual-mode hybrid architecture based on the practical observations. We design the system with the realistic operating condition of the electric vehicles and present the feasibility of the proposed method. The experimental result shows that the proposed dual-mode hybrid architecture is able to maintain the temperature of the battery within a pre-determined safe range with the benefit of discharging time extension or capacity fade reduction.

REFERENCES

[1] U.S. Department of Energy, "Automotive li-ion battery cooling requirements," 2012. http://www.eere.energy.gov.
[2] D. Brooks and et al., "Dynamic thermal management for high-performance microprocessors," in *HPCA*, 2001.
[3] D. Shin and et al., "Energy-optimal dynamic thermal management: Computation and cooling power co-optimization," *IEEE TII*, 2010.
[4] D. Shin and et al., "Constant-current regulator-based battery-supercapacitor hybrid architecture for high-rate pulsed load applications," *Journal of Power Sources*, 2012.
[5] A. Millner, "Modeling lithium ion battery degradation in electric vehicles," in *CITRES*, 2010.
[6] T. Yuksel and et al., "Evaluation of the effects of thermal management on battery life in plug-in hybrid electric vehicles," in *Battery Congress*, 2012.
[7] M. Zolot and et al., "Thermal evaluation of toyota prius battery pack," in *Future Car Congress*, 2002.
[8] A. Pesaran and et al., "Cooling and preheating of batteries in hybrid electric vehicles," in *AJTEC*, 2003.
[9] S. Pay and et al., "Effectiveness of battery-supercapacitor combination in electric vehicles," in *IEEE Bologna Power Tech Conference*, 2003.
[10] G. Sikha and B. N. Popov, "Performance optimization of a battery-capacitor hybrid system," *Journal of Power Sources*, 2004.
[11] C. E. Holland and et al., "Experimental characterization of hybrid power systems under pulse current loads," *Journal of Power Sources*, 2002.
[12] S. Chen and et al., "Thermal analysis of lithium-ion batteries," *Journal of Power Sources*, 2005.
[13] T. D. Hatchard and et al., "Thermal model of cylindrical and prismatic lithium-ion cells," *Journal of The Electrochemical Society*, 2001.
[14] H. Maleki and et al., "Thermal properties of lithiumion battery and components," *Journal of The Electrochemical Society*, 1999.
[15] R. P. Stout, "General thermal transient rc networks," 2006. ON Semiconductor.
[16] D. Shin and et al., "Online estimation of the remaining energy capacity in mobile systems considering system-wide power consumption and battery characteristics," in *ASP-DAC*, 2013.
[17] Sony Corporation, "Lithium Ion Rechargeable Batteries Technical Handbook."
[18] M. Petricca and et al., "An automated framework for generating variable-accuracy battery models from datasheet information," in *ISLPED*, 2013.
[19] Q. Xie and et al., "State of health aware charge management in hybrid electrical energy storage systems," in *DATE*, 2012.
[20] T. Yuksel and et al., "Evaluation of the effects of thermal management on battery life in plug-in hybrid electric vehicles," in *Society of Automotive Engineers World Congress*, 2012.
[21] Texas Instrument, "LM3641 Lithium-Ion Battery Pack Protection Circuit," 2011.
[22] Maxwell technologies, "Datasheet: Ultracapacitor cell integration kit."
[23] Maxwell technologies, "Datasheet: Bc series ultracapacitors."
[24] U.S. Environmental Protection Agency, "Emission Standards Reference Guide: EPA US06 or Supplemental Federal Test Procedure (SFTP)." http://www.epa.gov/.
[25] K. W. Matthew and et al., "Advisor 2.0: A second-generation advanced vehicle simulator for systems analysis," in *NAEVI*, 1999.
[26] R. Sadoun and et al., "Sizing of hybrid supply (battery-supercapacitor) for electric vehicle taking into account the weight of the additional buck-boost chopper," in *REVET*, 2012.
[27] L. Gao and et al., "Dynamic Lithium-ion battery model for system simulation," *IEEE TCPT*, 2002.
[28] Vishay Siliconix, "SiR422DP N-Channel 40-V (D-S) MOSFET," 2009.